Results in Physics 73 (2025) 108240

Contents lists available at ScienceDirect

Results in Physics

journal homepage: www.elsevier.com/locate/rinp

Non-Fourier heat transfer analysis of sandwich conical shells with GPLs reinforced face sheets and porous core under moving heat flux

Yasin Heydarpour [a], Parviz Malekzadeh [a,*], Hanxing Zhu [b,*], Morteza Mohammadzaheri [c]

[a] Department of Mechanical Engineering, School of Engineering, Persian Gulf University, Bushehr 7516913798, Iran
[b] School of Engineering, Cardiff University, Cardiff CF24 3AA, UK
[c] Engineering Department, German University of Technology, Halban 130, Oman

ARTICLE INFO

Keywords:
Sandwich conical shells
Nanocomposite face sheets
Porous core
Non-Fourier heat transfer
Moving heat flux
Graphene platelets

ABSTRACT

In this work, as a first attempt, the thermal behavior of nanocomposite sandwich conical shells under internal axisymmetric moving heat flux based on the non-Fourier heat transfer is investigated. In order to capture the influences of the finite heat wave speed, the hyperbolic heat transfer equation is used. The face sheets of the nanocomposite sandwich shell are made of graphene platelets (GPLs) reinforced polymer matrix. The core layer is fabricated from a GPLs reinforced porous composite material. In both core layer and face sheets, GPLs have uniform distribution and random orientation. Through a two-dimensional layerwise approach, the differential quadrature method (DQM) and the nonuniform rational basis spline (NURBS) curves based multi-step technique are employed to discretize the governing equations in the spatial and temporal domains, respectively. The performance of the present method is demonstrated by performing convergence study and comparing the results in the limit cases with those reported in literature. Following the approach validation, parametric studies are carried out to elucidate the influences of heat flux speed, porosity distribution and amounts, GPLs weight fractions and the shell-thickness-to-length ratio on the thermal responses of the sandwich conical shells under investigation. The results show that the speed of moving heat flux and GPLs weight fractions have significant effects on the thermal responses of the shells. But the porosity distribution and amounts have less effect on the thermal behavior of the shell. In addition, the increase of the heat flux speed decreases the traveled distance by the heat wave front and the increase of the weight fraction of GPLs increases the heat wave speed.

Introduction

Truncated conical and cylindrical shells are widely used in aerospace engineering, marine engineering, civil and mechanical engineering, for example, in aircraft propulsion systems, underwater vehicles, spacecraft, missiles and reactors [1–9]. In most cases, these structural elements must withstand high temperature changes and mechanical stress while minimizing their weight and maximizing their structural performance. On the other hand, the increasing demand for high-performance composites has aroused great interest in characteristics such as high strength and stiffness to weight ratios, high fatigue life, low cost, tailor-made properties, for use in modern industries like aerospace. Heat transfer is fundamental in many industrial applications of composite shells. In such applications, accurately predicting the thermal behavior of the truncated conical shells made of advanced composites under varying temperature conditions is crucial for design and manufacturing [10].

In recent years, advancements in manufacturing technologies, especially the creation of 3D printing [11], have allowed the construction of advanced new composite materials by using nanofillers. These advancements have improved thin-walled structures so as to survive harsh conditions. Carbon nanotubes (CNTs), graphene and its derivatives are the most widely used nanofillers to fabricate advanced polymer-based nanocomposites in recent years [12–19]. In comparison with CNTs, graphene is a extensively available nanomaterial with relatively low cost and excellent mechanical properties [20]. Also, due to their larger contacting surface area and the stronger bonding with the matrix, GPLs provide more reinforcing effects than CNTs [21,22]. These interesting properties have made the graphene one of the most promising nano-reinforcement material to be used to produce high performance advanced composite materials [23,24]. On the other hand, the existence of pores in composite materials, either purposeful or

* Corresponding authors.
E-mail addresses: malekzadeh@pgu.ac.ir, p_malekz@yahoo.com (P. Malekzadeh), zhuh3@cardiff.ac.uk (H. Zhu).

https://doi.org/10.1016/j.rinp.2025.108240
Received 30 January 2025; Received in revised form 23 March 2025; Accepted 29 March 2025
Available online 5 April 2025

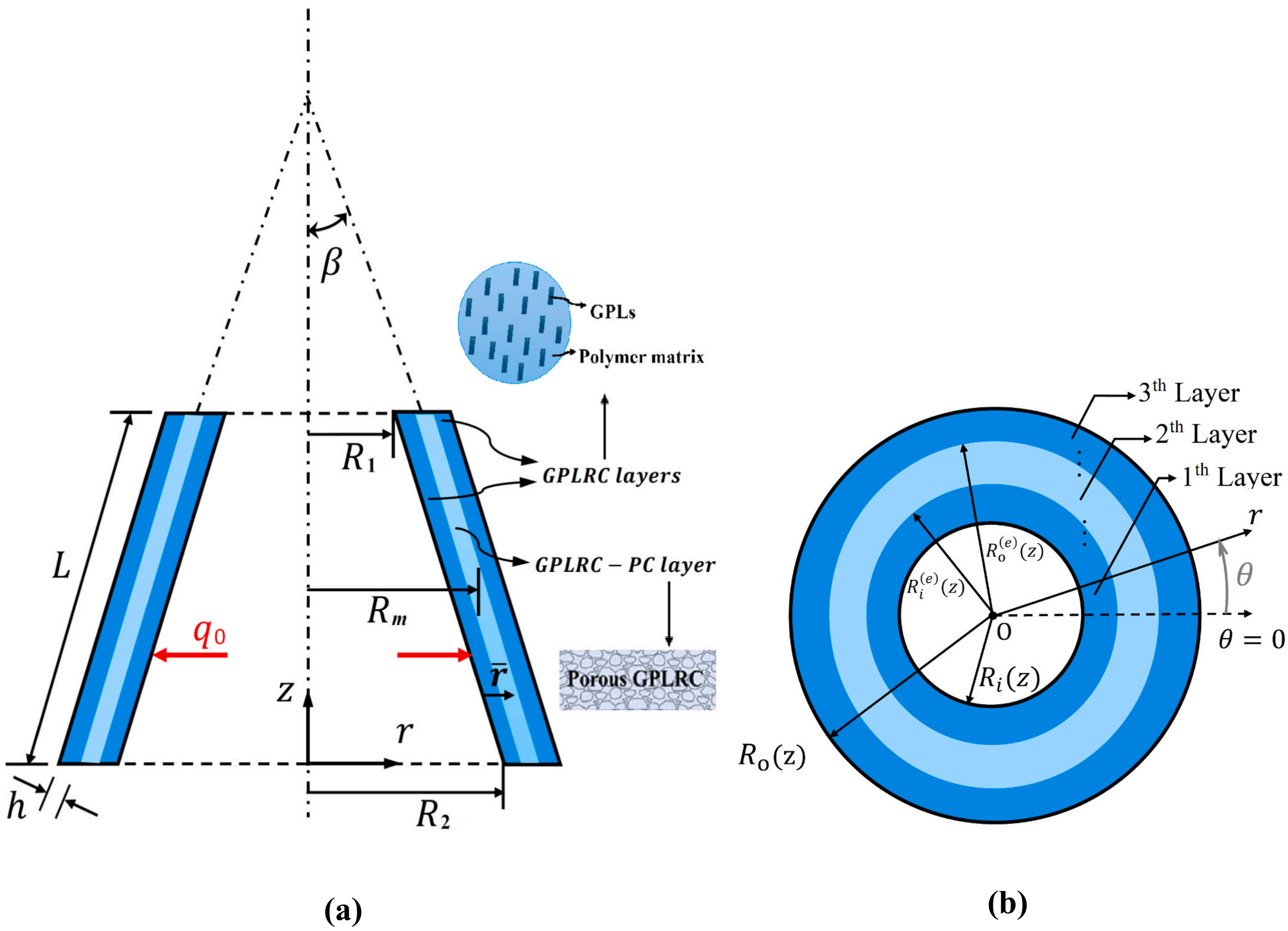

Fig. 1. The geometry and coordinate system of multilayer GPLRC truncated conical shell.

unintended, lowers the overall stiffness of the constructed composite structure. However, adding small amounts of GPLs to the base material, remarkably compensates this drop in stiffness [25–37]. In addition to their stiffness, GPLs can also effectively increase the thermal conductivity of reinforced nanocomposites [38].

Expectedly, the heat conduction analysis of multi-layer and composite materials is more complicated than that of one-layer homogeneous isotropic media [39–42]. In spite of its merits, analytical solutions are limited to problems with relatively simple geometries and boundary conditions. Consequently, to handle the complicated heat transfer problems of nanocomposite structures, the use of efficient and accurate numerical methods become essential for their in-depth study.

There are some research works concerning the heat transfer analysis of cylindrical and conical shells made of different materials. Here, some recent ones are reviewed briefly. Amiri Delouei et al. [43] employed a combination of Laplace transform, Fourier transform, and meromorphic functions to present an analytical solution for the two-dimensional axisymmetric conduction heat transfer analysis of a functionally graded (FG) cylindrical shells. Tokovyy et al. [44] proposed an analytical technique to analyze the two-dimensional steady state temperature distributions in laminated hollow cylinders composed of layers with different materials. In another work, Tokovyy [45] analytically estimated two-dimensional steady state temperature distributions in a radially FG cylindrical shell. In both these works, it was assumed that the temperature varies along the radial and circumferential directions only.

Norouzi and Rahamani [46,47] developed analytical solutions for the two-dimensional heat conduction transfer analysis of anisotropic conical shells by employing appropriate transformation and the separation of variables method. Erfan Manesh et al. [48,49] analytically investigated two-dimensional steady and unsteady conduction heat transfer in heterogeneous anisotropic composite conical shells with temperature-dependent thermal conductivities. Heydarpour and Aghdam [50] introduced a new multistep technique based on the NURBS curves to analyze the nonlinear transient heat transfer of functionally graded truncated cone under conventional thermal boundary conditions. In another study, Heydarpour and Malekzadeh [51] numerically performed the three-dimensional heat transfer analysis of multilayer functionally graded GPLs reinforced composite truncated conical shells subjected to stationary thermal boundary conditions based on non-Fourier conduction heat transfer law. Huang et al. [52] established a heat transfer model for a multilayer composite cylinder with porous media in the context of Fourier's law and validated the proposed model by designing an experiment. Duan et al. [53], through the use of simplifying assumptions and reduction of three-dimensional heat transfer equation to a one-dimensional one, analyzed the transient heat conduction within a conical probe surrounded by a semi-infinite thermal medium. Then, they used Laplace transform and solved the resulting ordinary differential equation. Amiri Delouei et al. [54] presented a two-dimensional analytical solution to estimate the temperature distribution in a functionally graded conical shell. Mohammadlou et al. [55] studied the steady state axisymmetric thermoelastic responses of a thin-walled conical shell subjected to uniform heat flow along its side surfaces. They assumed there are thermal insulation at both ends of shell and utilized the Galerkin finite element method to solve the semi-coupled steady state thermoelastic equations.

The literature review indicates that the thermal analysis of the sandwich truncated conical shells with GPLs reinforced face sheets (GPLR-FS) and porous core (GPLR-PC) subjected to moving heat flux is not investigated yet. These types of thermal problems have both academic value and industrial applications. On the other hand, it is well known that the classical Fourier heat conduction law cannot capture the effect of finite value of heat wave speed in thermal problems with suddenly applied thermal loadings. Hence, it cannot predict the conduction heat wave propagation and also an accurate estimation of the temperature in the structures under such a thermal loadings. Therefore, this study aims to undertake a comprehensive analysis of the non-Fourier thermal characteristics of these types of advanced structures under complex thermal conditions. For this purpose, a layerwise approach is employed to derive the non-Fourier heat conduction equations of each layer of the sandwich truncated conical shells. The thermal compatibility conditions at the interface of the adjacent layers are implemented exactly. Also, the external boundary conditions are satisfied at the inner and outer surfaces together with the ends of the shell. With the proposed numerical method, the strong form of these conditions at the boundaries and the layer interfaces and the non-Fourier heat conduction equations at the interior points of the shell layers are discretized. The validity of the proposed approach is demonstrated through its convergence behavior and comparison with existing solutions in the limit cases. Then, the effects of the heat flux speed, porosity distribution and amounts, GPLs weight fractions and the shell-thickness-to-length ratio on the thermal responses of the sandwich truncated conical shells with GPLs reinforced face sheets and porous core are presented and discussed.

Mathematical simulation

The sandwich conical shell under investigation has three perfectly bonded co-axial layers and is shown in Fig. 1. As illustrated in this figure, the core layer is made of a porous material, which is reinforced by GPLs. Also, the face sheets are built from a GPLs reinforced polymer matrix. In each layer, the GPLs are continuously and evenly distributed throughout its thickness. A coordinate system r-θ-z θ is used to signify the material points of the shell (see Fig. 1 (a) and (b)). The geometric parameters of the shell, including its length L, smallest inner radius R_1, largest inner radius R_2, the semi-apex angle β, mean radius R_m (at the section $z = 0.5L\cos\beta$) and layer thickness h, are shown in Fig. 1 (a). The formulation for the estimation of the effective material properties and the fundamental equations based on the non-Fourier heat conduction are presented in the next section.

The estimation of shell layers material properties

Due to low variation of the mass density and specific heat capacity of the nanocomposite materials resulted from reinforcing an isotropic polymer matrix by GPLs, their equivalent values are evaluated using the rule of mixture. Accordingly, the equivalent mass density ρ and specific heat capacity c of the face sheets are formulated as [51]

$$\rho = \rho_m V_m + \rho_{GPL} V_{GPL} \tag{1}$$

$$c = c_m V_m + c_{GPL} V_{GPL} \tag{2}$$

where V_{GPL} and V_m represent the GPLs and matrix volume fractions of the shell layer, respectively, which obey the relation $V_{GPL} + V_m = 1$. Thus, the subscripts m and GPL denote the matrix and GPLs. In order to simplify the realization and calculation of the GPLs volume fraction, it is expressed in terms of its weight fraction W_{GPL} as

$$V_{GPL} = \frac{W_{GPL}}{W_{GPL} + (\rho_{GPL}/\rho_m)(1 - W_{GPL})} \tag{3}$$

However, the effective thermal conductivity is estimated using the relation introduced by Chu et al. [56,57]

$$\frac{k}{k_m} = \frac{2/3\,(V_{GPL} - 1/\chi)^{\gamma}}{H(\chi) + 1/(k_{GPL}/k_m - 1)} + 1 \tag{4}$$

where γ is a fitting parameter and $\chi = a_{GPL}/t_{GPL}$ in which a_{GPL}, b_{GPL} and t_{GPL} are the GPLs length, width and thickness, respectively. In addition, the function $H(\chi)$ has the following definition [56,57]

$$H(\chi) = \frac{\ln\left(\chi + \sqrt{\chi^2 - 1}\right)\chi}{\sqrt{(\chi^2 - 1)^3}} - \frac{1}{\chi^2 - 1} \tag{5}$$

The existence of porosities in the core layer affects its material properties. The porosity density changes in the thickness direction have been more reported than those in other directions in the literature. In this study, the same FG porosity distribution patterns that have been usually used in the previous researches are considered. Accordingly, the effective thermal conductivity (k), specific heat capacity (c) and density (ρ) of the porous core are approximated as

$k(r) = k_c[1 - \Xi(r, e_0)]$, $c(r) = c_c[1 - \Xi(r, e_0)]$, $\rho(r) = \rho_c[1 - \Xi(r, e_m)]$ (6a-c).

where k_c, c_c and ρ_c are the effective thermal conductivity, specific heat capacity and density of the GPLR core without porosity (a perfect one), respectively. Also, the porosity functions $\Xi(z, e_0)$ for each of the three types of porosity distribution patterns are as follows [35,37].

Type 1: $\Xi(z, e_\alpha) = e_\alpha \cos[\pi(0.5 - \bar{r})]$
Type 2: $\Xi(z, e_\alpha) = 1 - e_\alpha \cos[\pi(0.5 - \bar{r})]$
Type 3: $\Xi(z, e_\alpha) = e_\alpha \cos(0.5\bar{r}\pi)$ (7a-c).

where $\alpha = 0, m$ and $\bar{r} = \left[\frac{r - R_i(z)}{h\sec\beta}\right]$, which indicates $0 \le \bar{r} \le 1$. Also, $e_\alpha(\alpha = 0, m)$ is the porosity coefficient and are determined as [35,37]

$$e_m = 1 - \frac{\rho_{\min}}{\rho_c} \tag{8}$$

where $\rho_{\min}$ is the minimum value of the GPLR porous core density. e_m can be related to e_0 as

$$e_m = 1 - \sqrt{1 - e_0} \tag{9}$$

In this work, to perform rational studies with different porosity distribution patterns, the same values for the masses of the GPLR porous cores are considered.

Non-Fourier heat conduction equations

Neglecting the internal heat generation source and based on the hyperbolic heat transfer, the following equations present the constitutive transfer equation and the balance of energy principle for each nanocomposite layer of the sandwich shell respectively [51]

$$\tau_0 \frac{\partial \vec{q}}{\partial t} + \vec{q} = -k\vec{\nabla} T \tag{10a}$$

$$\rho c \frac{\partial T}{\partial t} = -\vec{\nabla}.\vec{q} \tag{10b}$$

where $T[= T(r, z, t)]$ represents the temperature, $\vec{q}(r, z, t)$ the heat flux vector at an arbitrary material point (r, θ, z), t time, τ_0 the relaxation time and $\vec{\nabla}$ the three-dimensional gradient vector in the cylindrical coordinate system, respectively. Using Eq. (10a) to remove $\vec{q}$ from Eq. (10b), the result becomes

$$\frac{1}{r}\frac{\partial}{\partial r}\left(rk\frac{\partial T}{\partial r}\right) + \frac{\partial}{\partial z}\left(k\frac{\partial T}{\partial z}\right) = \rho\, c\left(\frac{\partial T}{\partial t} + \tau_0\frac{\partial^2 T}{\partial t^2}\right) \tag{11}$$

A circumferentially uniform moving ring heat flux is assumed to be applied on the inner surface of the sandwich shell.

At $r = R_i$: $-k\frac{\partial T}{\partial r} = q_0\,\delta(z - z_0(t))$ (12).

where q_0 and z_0 are the strength and the position of the moving heat flux along the z-axis, respectively. Also, the symbol $\delta(\,)$ represents the Dirac delta function. In this study, without loss of the generality of the

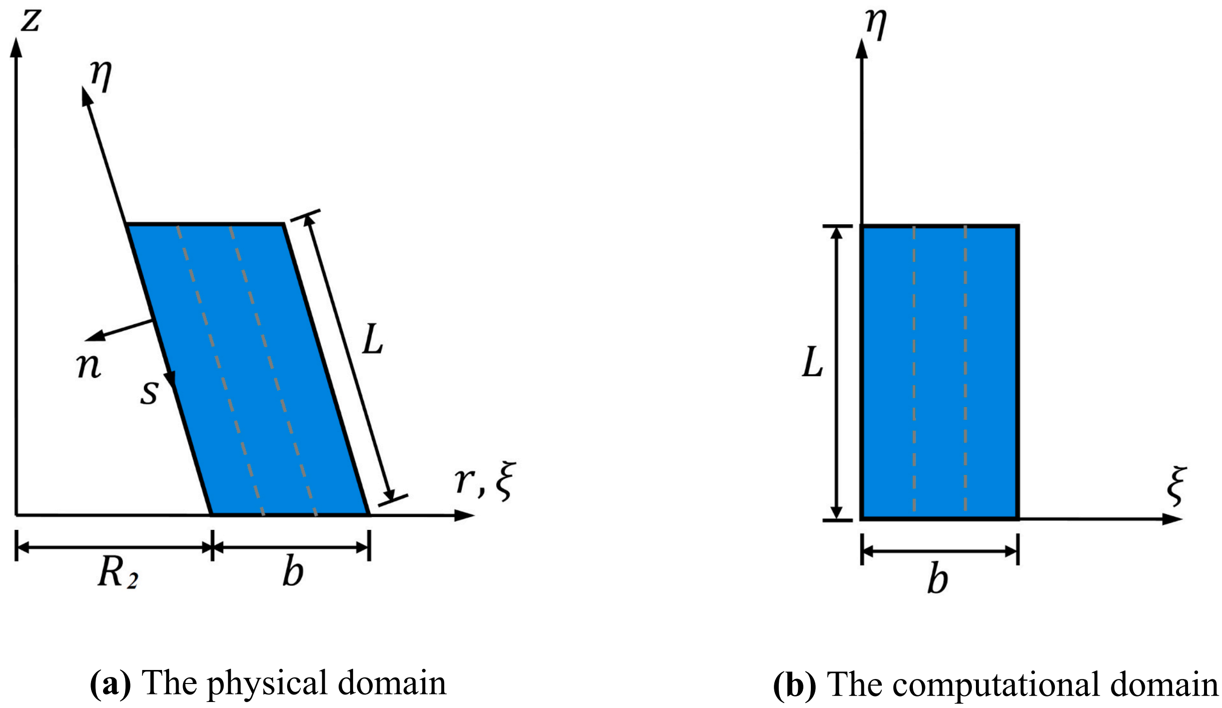

Fig. 2. The physical and computational domains.

solution technique, it is assumed that the heat flux moves with a constant speed u along the z-axis and enters the shell at time $t = 0$. Therefore, it can be written as $z_0(t) = ut$ in Eq. (12).

Along the shell outer surface, the convection heat transfer is assumed to take place. Therefore.

At $r = R_o$: $-k\frac{\partial T}{\partial r} = h_c(T - T_\infty)$ (13).

where T_∞ and h_c are the shell outer media temperature and the convection heat transfer coefficient, respectively.

Without any restriction due to the formulation and solution technique, the isolation thermal conditions are assumed on the ends of the shell surfaces (i.e., $z = 0$ and $z = L\cos\beta$).

At $z = 0$ and $z = L\cos\beta$: $\frac{\partial T}{\partial z} = 0$ (14a,b).

Also, the initial thermal conditions are assumed to be.

$T(r, z, 0) = T_0, \left.\frac{\partial T(r,z,t)}{\partial t}\right|_{t=0} = 0$(15a,b).

In addition to the mentioned thermal boundary conditions on the shell surfaces which are due to environmental effects, the following thermal compatibility conditions at the interface of two adjacent layers of the truncated conical sandwich shells must be fulfilled.

$T\left(R_o^{(e)}, t\right) = T\left(R_i^{(e+1)}, t\right), k\left.\frac{\partial T}{\partial r}\right|_{r=R_o^{(e)}} = k\left.\frac{\partial T}{\partial r}\right|_{r=R_i^{(e+1)}}$ for $e = 1, 2, 3$ (16a, b).

where $e = 1$, 2 and 3 signify the inner face sheet, the core layer and the outer face sheet layer of the sandwich shell, respectively.

Solution technique

Due to complicated shell geometry and the non-Fourier heat transfer equation (11) subjected to the prescribed boundary and compatibility thermal conditions, it is very difficult to obtain the corresponding solution analytically. Therefore, in this work, a combined numerical technique is employed to get the solution, which is briefly reviewed in the next subsection. The DQM based on the direct projection of the Heaviside function [58] is utilized to discretize the governing equations in the spatial domain (detailed in subsections 3.1). Then, the resulting system of differential equations are solved in time domain using NURBS based on a multi-step technique [59,60], details of which are presented in subsections 3.2.

Spatial discretization: DQM-Heaviside function

To present a computationally efficient and accurate solution technique, the DQM based on the direct projection of the Heaviside function together with the NURBS based multi-step method technique is employed to obtain the temperature distribution in the sandwich conical shell with nanocomposite face sheets and pros core [58–60]. Accordingly, the governing equations are discretized in the spatial domain and transformed into time domain as a system of initial value differential equations.

Since the computational domain of the DQM is a rectangular one, a transformation between the physical domain (i.e., the skewed cross section of the nanocomposite shell layer) and the computational domain is required. This can be easily done by employing the following geometric relations that map the skewed quadrilateral cross-section of the shell into a rectangular one

$$r = R_2 + \xi - \eta\sin\beta, z = \eta\cos\beta \quad (17)$$

where ξ and η denote the variables of coordinate system in the computational domain (see Fig. 2). Now, each of the transformed face sheets and the core layers are discretized into N_ξ and N_η grid points in the $\xi-$ and $\eta-$directions, respectively. According to the DQM, the resulting non-Fourier heat conduction (11) is employed and discretized at the domain grid points in each layer. In addition, the external boundary conditions and interface compatibility conditions are discretized exactly at the corresponding boundary and interface grid points. To reduce the paper length, the DQM discretization procedure is only applied to Eq. (11) and after that it takes the following form $k_{ij}(1 + \tan^2\beta)\sum_{m=1}^{N_\xi} B_{im}^{\xi} T_{mj} + \left[(1 + \tan^2\beta)\left(\frac{\partial k_{ij}}{\partial \xi}\right)_{ij} + \frac{k_{ij}}{R_2 + \xi_i - \eta_j\sin\beta}\right]\sum_{m=1}^{N_\xi} A_{im}^{\xi} T_{mj} + k_{ij}\sec^2\beta\sum_{n=1}^{N_\eta} B_{jn}^{\eta} T_{in}$

$$+\sec\beta\tan\beta\left(\frac{\partial k_{ij}}{\partial\xi}\right)_{ij}\sum_{n=1}^{N_\eta}A_{jn}^{\eta}Tk_{in}+2k_{ij}\tan\beta\sec\beta\sum_{m=1}^{N_\xi}\sum_{n=1}^{N_\eta}A_{im}^{\xi}A_{jn}^{\eta}T_{mn}$$
$$=\rho_{ij}c_{ij}\left(\frac{dT_{ij}}{dt}+\tau_{0ij}\frac{d^2T_{ij}}{dt^2}\right) \quad (18)$$

where A_{ij}^{α} and $B_{ij}^{\alpha}(\alpha=\xi,\eta)$ represent the first and second-order DQM weighting coefficients of the $\alpha-$direction, respectively [51]. After completing the DQM discretization procedure of Eq. (11) in all the three sandwich shell layers and the related boundary and interfacial compatibility conditions, one gets a system of initial value differential equations, which can be represented in the matrix form as

$$\mathbf{M}\frac{d^2\widehat{\mathbf{T}}}{dt^2}+\mathbf{C}\frac{d\widehat{\mathbf{T}}}{dt}+\mathbf{K}\widehat{\mathbf{T}}=\mathbf{f} \quad (19)$$

where $\widehat{\mathbf{T}}$ is the vector of unknown temperature at all grid points; also, $\mathbf{M}$, $\mathbf{C}$ and $\mathbf{K}$ are the coefficient matrices and the load vector is denoted by $\mathbf{f}(t)$. The components of these matrices and vector are derived through the discretized form of Eqs. (11)-(14) and (16).

Temporal discretization: The NURBS based multi-step method

At this stage, a suitable numerical technique should be adopted to solve the system of ordinary differential equations (19) subjected to the corresponding initial conditions. This task can be performed using the traditional numerical methods such as those of the finite difference-based schemes, for example Newmark's time integration family, or other recently proposed ones [61–71]. However, it has been shown that the time integration scheme developed based on the NURBS curves has better performance over Newmark's method [50,65,67–71]. In order to apply this technique for solving the system of second-order differential equations (19), these equations can be broken down into a set of the first-order ones.

$$\begin{cases}\dfrac{d\widehat{\mathbf{T}}}{dt}=\psi\\ \mathbf{M}\dfrac{d\psi}{dt}+\mathbf{C}\psi+\mathbf{K}\widehat{\mathbf{T}}=\mathbf{f}\end{cases} \quad (20a,b).$$

where $\psi=\widehat{\mathbf{T}}$. It should be mentioned that when using this method, the various schemes can be generated by only varying the weighting coefficients (w_i) and/or the order of NURBS curves. In the current work, the four-step scheme, which has the following weight coefficients [50,51], is chosen to solve Eqs. (20a,b).

$w_1=0.001, w_2=0.001, w_3=2$ and $w_4=3$ (21a-d).

Based on this approach, the set of these ordinary differential equations is transformed into the following system of explicit algebraic equations, respectively

$$\widehat{\mathbf{T}}_{n+1}=\widehat{\mathbf{T}}_n+\Delta t(1.50002585\psi_n-0.50005291\psi_{n-1}+0.00002827\psi_{n-2}-0.00000120\psi_{n-3}) \quad (22)$$

$$\psi_{n+1}=\psi_n+\Delta t(1.50002585\widehat{\psi}_n-0.50005291\widehat{\psi}_{n-1}+0.00002827\widehat{\psi}_{n-2}-0.0000012\widehat{\psi}_{n-3}) \quad (23)$$

where Δt is the time step size and

$$\widehat{\psi}=\mathbf{M}^{-1}(-\mathbf{C}\psi-\mathbf{K}\widehat{\mathbf{T}}+\mathbf{f}) \quad (24)$$

When using this algorithm, to initiate the solution procedure, the values of the unknown vectors $\widehat{\mathbf{T}}$ and ψ at the first four steps of time increments must be known. In this regard, the values of the unknown vectors at the time $t=0$ are used as their values at the beginning of the procedure. Then, their values at the other three steps of time increments are estimated through the multi-step formulations. By continuing the procedure, Eqs. (20a,b) are discretized and changed to a set of algebraic equations, which can be solved easily using an existing standard solution technique. The output of this process is the values of the unknown vectors $\widehat{\mathbf{T}}$ and ψ at the end of each time step, which finally provides the time history of the temperature at the DQM grid points of each of the sandwich shell layers.

Table 1
Material properties of the epoxy and GPLs [68].

Material	Epoxy	GPLs
$\rho\ (\mathrm{kg/m^3})$	1200	1062.5
c (J/kgK)	1110	644
$\alpha\,(1/\mathrm{K})$	60×10^{-6}	5×10^{-6}
k (W/mK)	0.246	3000

Results and discussions

In this section, the presented approach is first validated and then, some parametric studies are conducted and discussed. The material properties of the matrix (i.e., epoxy) of the face sheets and GPLs are given in Table 1. Unless otherwise is specified, in presenting the numerical results, the following non-dimensional parameters are used to better generalize and interpret the results.

$Fo=\frac{tu}{L}, \tau=\sqrt{\frac{\tau_0\widehat{\alpha}}{R_m^2}}, T^*=\frac{h_c L^2}{q_0 h^2}, \zeta=\frac{\xi}{b}$ (25a-d).

where $\widehat{\alpha}(=k/\rho c)$ is the thermal diffusivity of the sandwich shells. In addition, if other values are not given, the geometric dimensions of GPLs [51] and the sandwich shell, and also the values of the thermal parameters are assumed to be

$$a_{GPL}=2.5\,(\mu\mathrm{m}), b_{GPL}=1.5\,(\mu\mathrm{m}), t_{GPL}=1.5\,(\mathrm{nm}), R_m=1\,(\mathrm{m}), L=1\,(\mathrm{m}), h=0.1\,(\mathrm{m}),$$

$$q_0=50000\left(\mathrm{W/m^2}\right)T_0=T_\infty=300(\mathrm{K})h_c=100\,(\mathrm{W/m^2K})$$

Verification

The correctness of formulation and accuracy of the solution method are verified by performing the convergence study and comparing the results with some existing results in the open literature. In this regard, the convergences of dimensionless temperature of the multilayer truncated conical shells with the GPLRC-FS and GPLR-PC against the number of time step N_t for both the NURBS based multi-step technique and Newmark's scheme are compared in Table 2. The results are provided for two different values of the dimensionless relaxation time. The fast rate of convergence of the NURBS based multi-step technique is observable. Also, it can be seen that the present multi-step method yields results with very little CPU time, which is almost o.1 % of the time spent when using the Newmark's time integration scheme.

The influences of the DQM grid points on the convergence of dimensionless temperature distribution along the shell thickness for the multilayer truncated conical shell with the GPLRC-FS and GPLRC-PC are presented in Fig. 3. The rapid convergence of the method when increasing the DQM grid points is quite evident. Based on these convergence studies, it is concluded that 200 time steps and 25 DQM gird points in each direction is sufficient to obtain the satisfactory converged results.

The approach is validated by analyzing a functionally graded cylinder under thermal environment and comparing the results with those reported in other references. The sandwich truncated conical shell is degenerated to cylindrical one by setting $\beta=0$. A comparative evaluation of results is performed with the solutions provided by Santos et al. [72]. They applied a semi-analytical finite element model to analyze the

Table 2
The convergence of dimensionless temperature of the multilayer truncated conical shell with the GPLRC-FS and GPLRC-PC using NURBS based multi-step technique and Newmark's scheme $[W_{GPL} = 1\%, \zeta = 0, \eta = 0.5, e_0 = 0.4$, porosity type 1, $\beta = 15^{o}, Fo = 1, u = 1\,(\mathrm{cm/s})]$.

τ		NURBS based multi-step method		Newmark's method	
	N_t	T^*	CPU time (s)	T^*	CPU time (s)
0.01	20	3.791	0.015894	4.526	6.447044
	60	4.548	0.021765	4.705	17.298792
	100	4.723	0.030194	4.762	28.312309
	200	4.814	0.061143	4.825	54.631392
	300	4.821	0.097584	4.828	86.849102
	400	4.821	0.136187	4.829	112.989265
0.03	20	3.813	0.013904	4.807	6.332125
	60	4.371	0.023760	4.982	17.892612
	100	4.846	0.028167	5.002	26.402607
	200	5.022	0.070849	5.031	57.846187
	300	5.030	0.094298	5.034	86.823790
	400	5.030	0.147328	5.034	114.123805

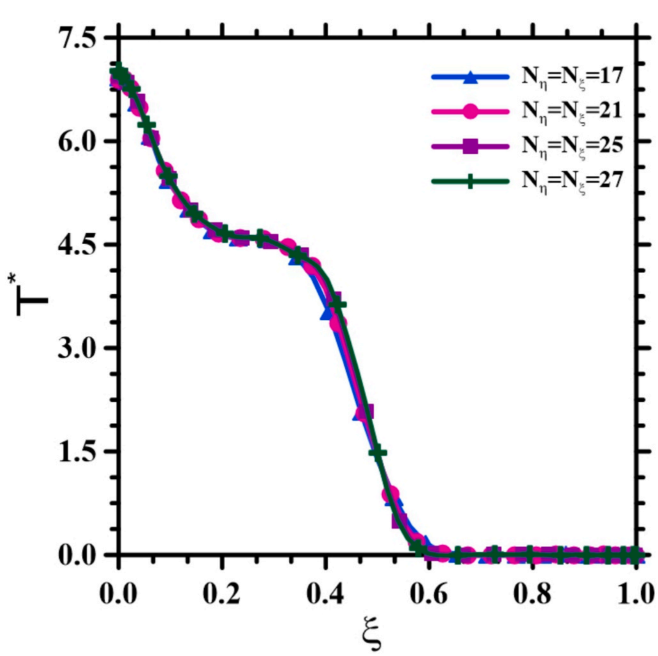

Fig. 3. The convergence of dimensionless temperature against the number of differential quadrature grid points for the multilayer truncated conical shell with the GPLRC-FS and GPLRC-PC $[W_{GPL} = 0.3\%, \eta = 0.5, e_0 = 0.4$, porosity type 1, $\beta = 15^{o}, Fo = 1, u = 1\,(\mathrm{cm/s}), \tau = 0.03]$.

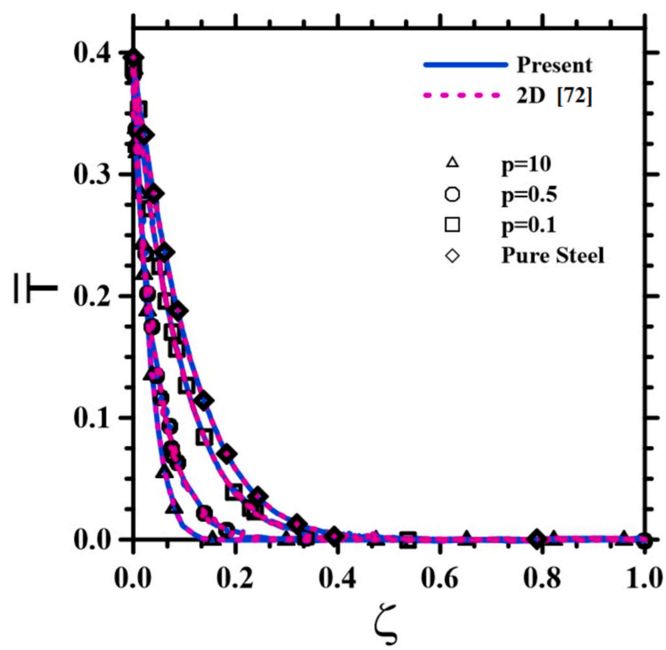

Fig. 4. Comparison of the dimensionless temperature distribution across the thickness of an FG hollow cylinder $[R_i = 4\,(\mathrm{cm}), R_o = 6\,(\mathrm{cm}), t = 1\,(\mathrm{s}), L = 20\,(\mathrm{cm}), \overline{T} = T/T_0, \eta = 0.5]$.

Table 3
Material properties of ceramic (Zirconia) and metal (steel) [72].

Material	Zirconia	steel
$k(\mathrm{W/cm^{\circ}C})$	2.09	20
$\rho(\mathrm{kg/m^3})$	5700	8166
$c(\mathrm{J/kg\ ^{o}C})$	531.9	325.35

FG cylindrical shells under the following thermal boundary and initial conditions based on the uncoupled classical thermoelasticity.

At $r = R_i$: $T(r, z, t) = T_0(1 - e^{-0.5t})$ (26a).

At $r = R_o$: $k\frac{\partial T}{\partial r} + h_c T = 0$ (26b).

At $z = 0,\ L$:$T(r, z, t) = 0$ (26c,d)

$$T(r, z, 0) = 0 \tag{26e}$$

Moreover, the material properties vary through the shell thickness from the ceramic at the inner surface to the metal at the outer surface along with the power law distribution as

$$P(r) = P_c + (P_m - P_c)V_m \tag{27}$$

where P denotes a generic material property and $V_m = \left(\frac{r - R_i}{R_o - R_i}\right)^p$ represents the volume fraction of the metal phase, in which p is the power law index, subscripts c and m signify the ceramic and metal materials, respectively. The material properties of metal and ceramic are given in Table 3. Fig. 4 shows the comparisons between the non-dimensional temperature distribution across the shell thickness for the two approaches and different values of the power law index p. The close agreement between the two approaches demonstrates the accuracy of the approach proposed in the current study.

In order to further show the accuracy of the present approach, the thermal analysis of an FG cylindrical shell with too large-to-diameter ratio for which the analytical solution exists, is presented. This example is chosen from Ref. [73], in which it was assumed that the thermal conductivity varies as

$$k = k_0 r^m \tag{28}$$

where m is the material graded index and k_0 is a constant material and a

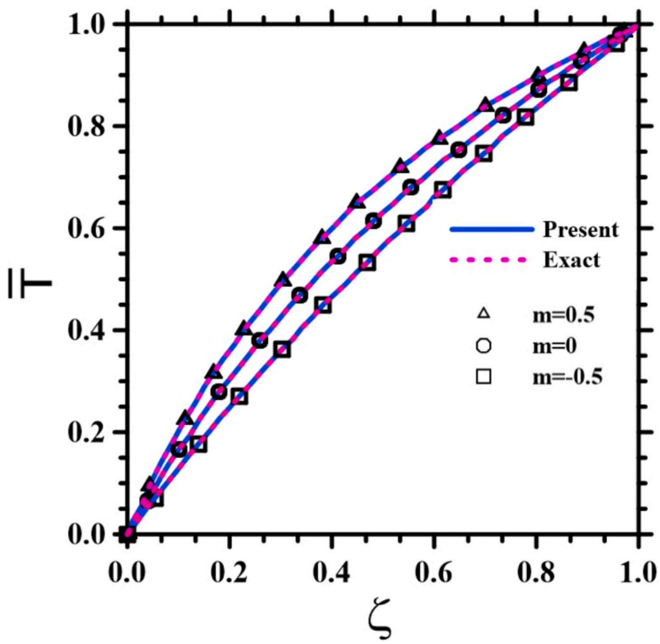

Fig. 5. Comparison of the dimensionless temperature in the FG hollow cylinder subjected to non-uniform temperature rise with exact solution ($R_i = 1, R_o/R_i = 3, L/R_i = 10, \overline{T} = T/T_0, \eta = 0.5$).

value of 2 (W/mK) is assumed for it in this example. The following thermal boundary conditions are employed at the inner and outer surfaces of the shell

$T(R_i) = 0$ °C, $T(R_o) = 100$ °C (29a,b).

The variations of the non-dimensional temperature along the FG shell thickness obtained using the present approach and those of the analytical solution are compared in Fig. 5. This comparison study is conducted for different values of the material graded index (m). The closeness of the results further indicates the high precision of this approach.

Parametric studies

From Eq. (11), it can be seen that the heat wave speed is equal to $\sqrt{\frac{k}{\rho c \tau_0}}$. Thus, by increasing the relaxation time, the heat wave speed must decrease. To verify this fact, the effect of dimensionless relaxation time on the dimensionless temperature of the sandwich truncated conical shell with the GPLRC-FS and GPLRC-PC is illustrated in Fig. 6. In Fig. 6(a), the variation of dimensionless temperature along the shell thickness direction is shown, meanwhile, in Fig. 6(b) the time history of dimensionless temperature at midpoint of the shell is exhibited. The results show that by increasing the dimensionless relaxation time, the distance traveled by the heat wave front reduces. This issue indicates that the heatwave velocity reduces by increasing the relaxation time, which verify the results predicted by the formulation given in the first line of this paragraph. The results also indicate that the used theory can detect the front of heat wave. As a results of the reduction of the heat wave speed, it can be seen from this figure that by increasing the dimensionless relaxation time, the maximum dimensionless temperature decrease (see Fig. 6(b)). Also, it can be observed that before reaching the steady state solution, the differences between the results are significant. These results also indicate the importance of non-Fourier heat transfer analysis for the problems with suddenly applied thermal loadings.

The impact of GPLs weight fraction on the through-the-thickness variation and time histories of the dimensionless temperature of the sandwich truncated conical shell with the GPLRC-FS and GPLRC-PC are presented in Fig. 7. It can be observed that increasing the weight fraction of GPLs increases the heat wave speed but decreases the maximum temperature. This is because the increase of the GPLs weight fraction increases the thermal conductivity considerably, but reduces both the mass density and specific heat capacity of the structure slightly. On the other hand, from the heat wave speed formulation (i.e., $\sqrt{\frac{k}{\rho c \tau_0}}$) it can be concluded that by increasing the thermal conductivity and decreasing the mass density and specific heat capacity, the heat wave speed increases. On the other hand, when increasing the GPLs weight fraction from zero to one percent, the mass density and specific heat capacity almost remain constant but the thermal conductivity increase up to 78 %. Consequently, by increasing the GPLs weight fraction, the maximum

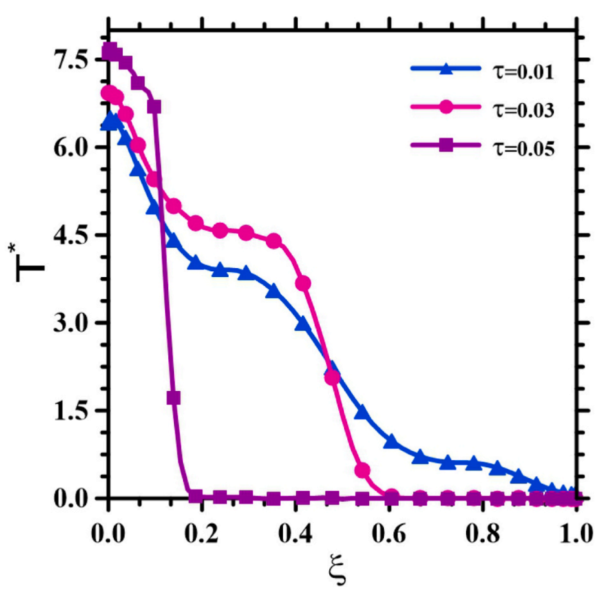

(a) $\eta = 0.5,\ Fo = 1$

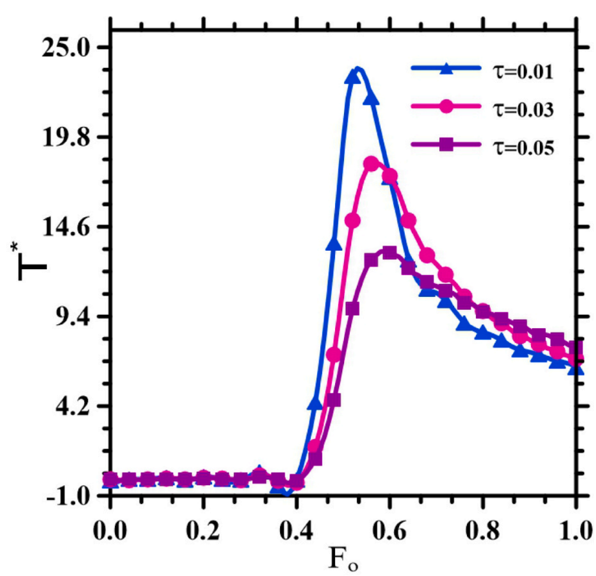

(b) $\zeta = 0, \eta = 0.5$

Fig. 6. The effect of nondimensional relaxation time on the nondimensional temperature of the sandwich truncated conical shell with the GPLRC-FS and GPLRC-PC [$W_{GPL} = 0.3\%, e_0 = 0.4$, porosity type 1, $u = 1$ (cm/s), $\beta = 15°$].

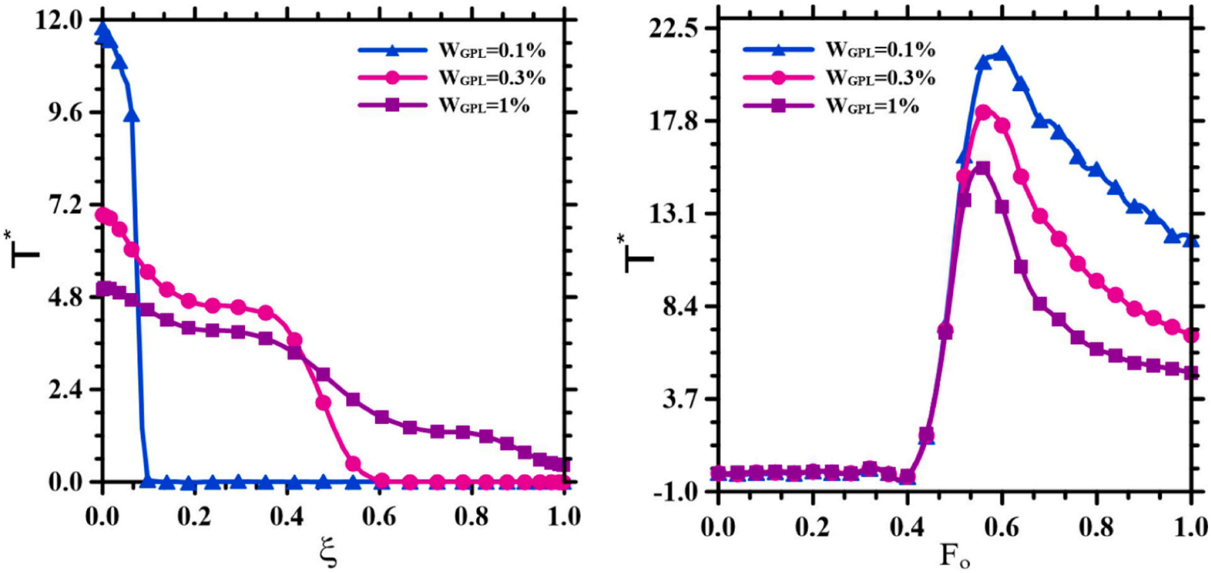

(a) $\eta = 0.5,\ Fo = 1$ **(b)** $\zeta = 0, \eta = 0.5$

Fig. 7. The effect of GPLs weight fraction on the through-the-thickness variation and time histories of the dimensionless temperature of the sandwich truncated conical shell with the GPLRC-FS and GPLRC-PC [$e_0 = 0.4$, porosity type 1,$\beta = 15^o$,$u = 1$ (cm/s), $\tau = 0.03$].

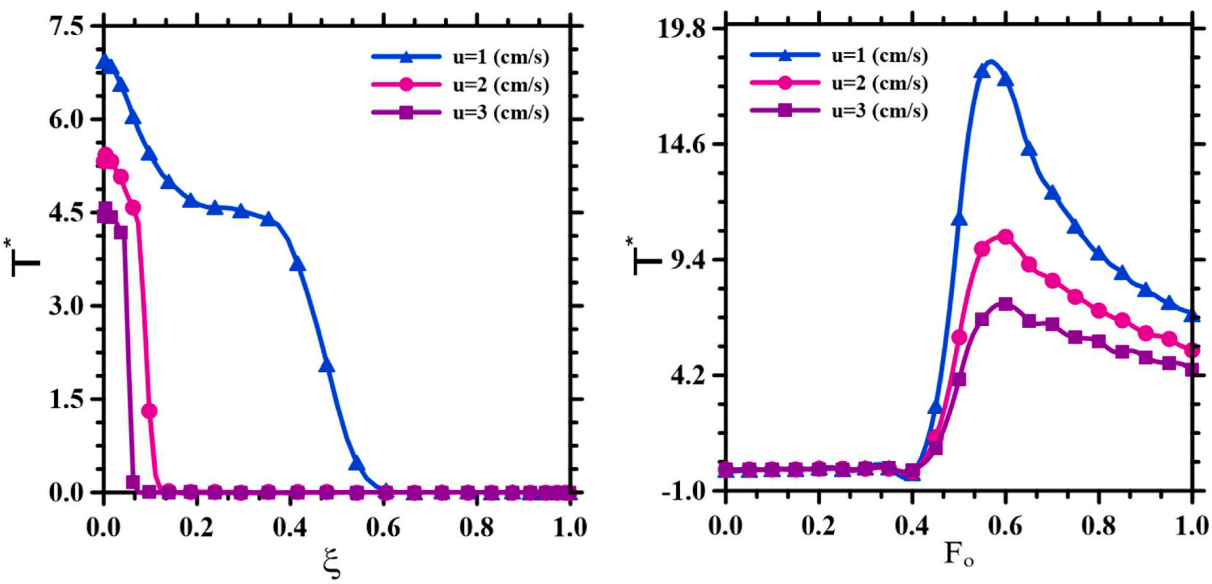

(a) $\eta = 0.5,\ Fo = 1$ **(b)** $\zeta = 0, \eta = 0.5$

Fig. 8. The influences of speed of the moving heat flux on the through-the-thickness variation and time histories of the dimensionless temperature of the sandwich truncated conical shell with the GPLRC-FS and GPLRC-PC ($W_{GPL} = 0.3\%, e_0 = 0.4$, porosity type 1,$\beta = 15^o$, $\tau = 0.03$).

temperature must decrease which verify the obtained results.

The influences of the speed of the moving heat flux on the through-the-thickness variation and time histories of the dimensionless temperature of the sandwich truncated conical shell with the GPLRC-FS and GPLRC-PC are depicted in Fig. 8. The results illustrate that the heat flux speed significantly affects the maximum values and the distribution of the dimensionless temperature. By increasing the heat flux speed, the heat wave front travels less distance at the same times. However, the time histories of the dimensionless temperature have the same trend of variations.

Figs. 9 and 10 present the effects of the porosity distribution and amounts on the thermal behavior of the sandwich shells under investigation, respectively. These figures indicate that both the porosity distribution and porosity amounts change the temperature distribution in the region traveled by the heat wave. However, they have no visible effect on the time histories of temperature at a specified point of the shell. This is due to the fact that the porosity distribution and amount do not change the thermomechanical properties of the sandwich shell under investigation considerably. The changes in the thermal conductivity, mass density and specific heat capacity of the shell are less than 2 percent when increasing the porosity amount parameter (i.e.,) from 0 to 0.6.

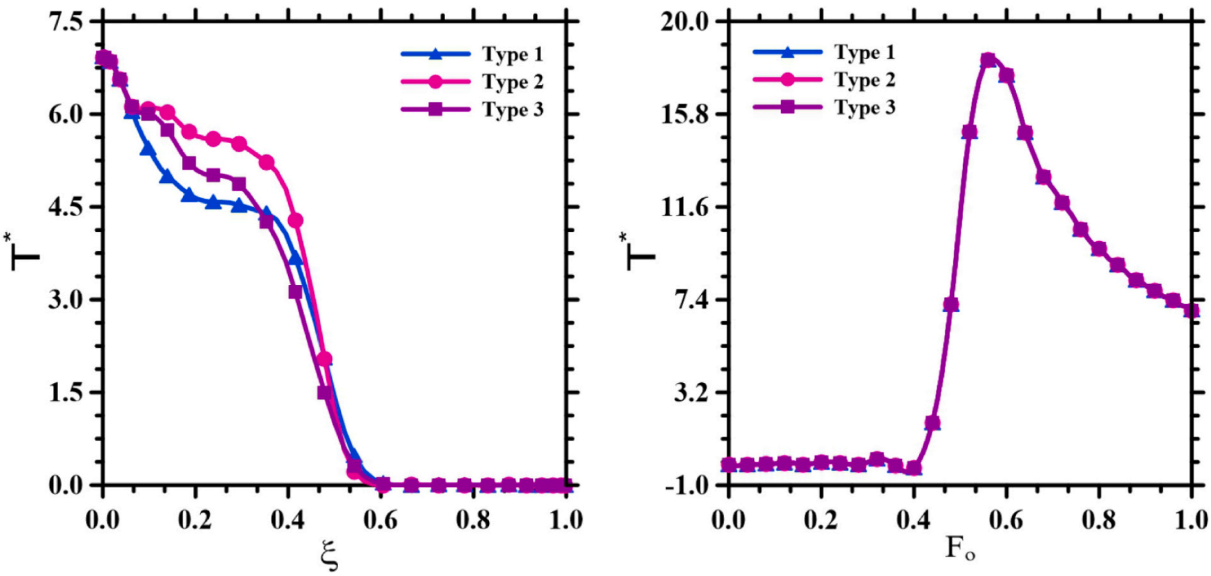

(a) $\eta = 0.5,\ Fo = 1$ (b) $\zeta = 0, \eta = 0.5$

Fig. 9. The effects of porosity distribution pattern on the through-the-thickness variation and time histories of the dimensionless temperature of the sandwich truncated conical shell with the GPLRC-FS and GPLRC-PC $[W_{GPL} = 0.3\%,\ e_0 = 0.4, \beta = 15^o,\ u = 1\,(\mathrm{cm/s}), \tau = 0.03]$.

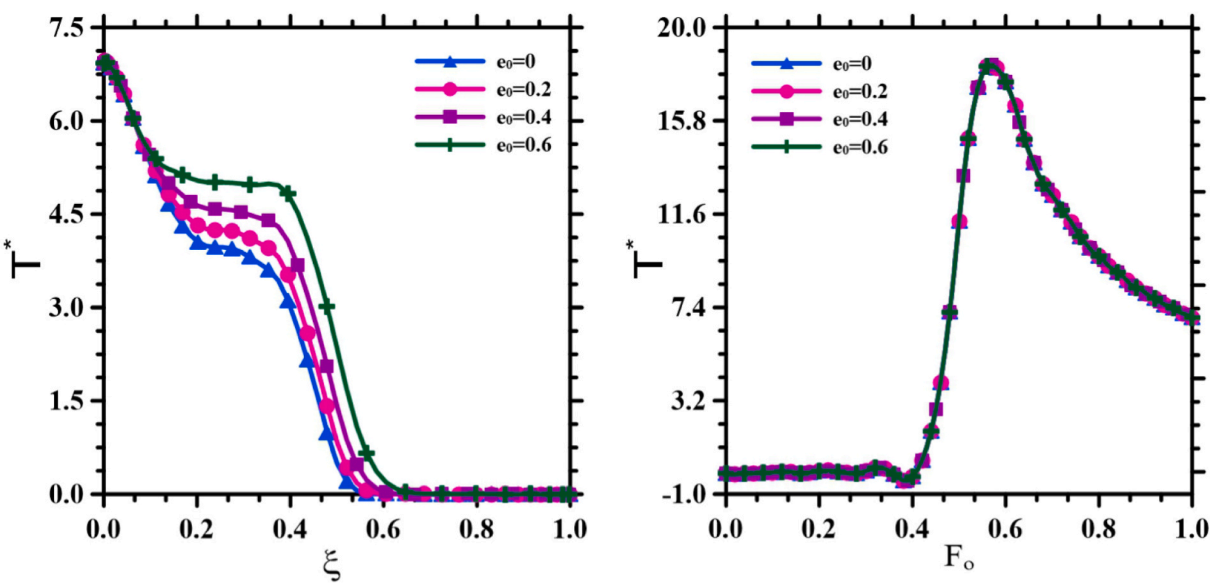

(a) $\eta = 0.5,\ Fo = 1$ (b) $\zeta = 0, \eta = 0.5$

Fig. 10. The effects of porosity amounts on the through-the-thickness variation and time histories of the dimensionless temperature of the sandwich truncated conical shell with the GPLRC-FS and GPLRC-PC $[W_{GPL} = 0.3\%,$ porosity type $1, \beta = 15^o,\ u = 1\,(\mathrm{cm/s}), \tau = 0.03]$.

Fig. 11 demonstrates that the shell thickness-to-length ratio affects both the temperature distribution along the shell thickness and the temperature time histories of a specified shell point. The results indicate that by increasing the shell thickness-to-length ratio, the maximum temperature under the same thermal boundary conditions decreases. Also, this geometric parameter significantly affects the temperature distribution and time history of temperature variations at material points of the sandwich shell under the same thermal boundary conditions.

Conclusion

As a first endeavor, the thermal responses of sandwich conical shells with GPLs reinforced face sheets and porous core subjected to internal axisymmetric moving heat flux were studied by considering a finite wave heat speed. In this regard, the hyperbolic heat transfer equation was used to model the conduction heat transfer in the shell. Both porous core layer and face sheets were reinforced by uniformly distributed and randomly orientated GPLs. A two-dimensional layerwise differential quadrature method and the nonuniform rational basis spline curves based multi-step technique were applied to spatially and temporarily

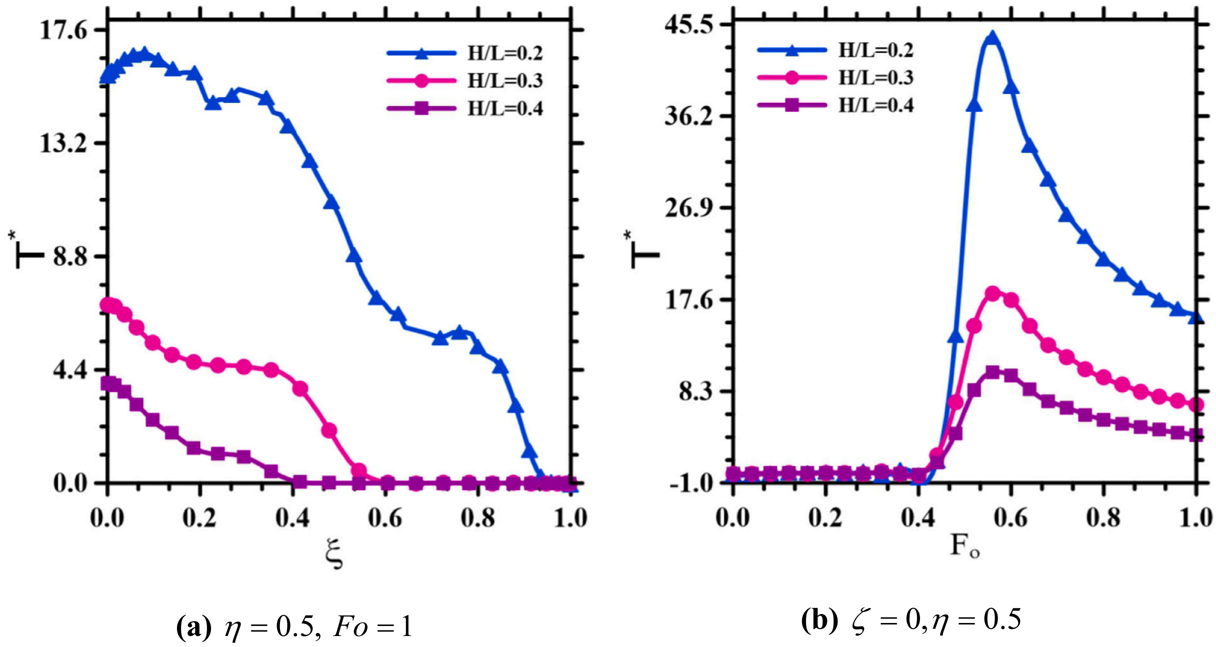

Fig. 11. The effects of the thickness-to-length ratio on the through-the-thickness variation and time histories of the dimensionless temperature of the sandwich truncated conical shell with the GPLRC-FS and GPLRC-PC [$W_{GPL} = 0.3\%,\ e_0 = 0.4$, porosity type 1,$\beta = 15^o$, $u = 1\,(\mathrm{cm/s}), \tau = 0.03$].

discretize the governing equations, respectively. The robustness and computational efficiency of this approach were illustrated by doing convergence and comparison studies. After that some parametric studies were conducted and the following observations were made.

- The increase of the dimensionless relaxation time reduces the dimensionless temperature and the heat wave speed.
- The speed of moving heat flux considerably changes the maximum values and the distribution of the dimensionless temperature. However, it did not change the trend of variations of time histories of the dimensionless temperature.
- The increase of the heat flux speed reduces the traveled distance by the heat wave front at the same times.
- The porosity distribution and amount affect the temperature distribution in the shell thickness but have no effect on the time histories of the temperature at a specified point of the sandwich shell.
- The increase of the shell thickness decreases the maximum temperature under the same thermal boundary conditions.

Because of its computational efficiency, the solution technique presented has strong potential for solving the iterative problems such as inverse ones. Also, the provided numerical results can be used as benchmark solution for the future research in the field. It should be mentioned that the problem with point moving heat source is a challenging one for the used solution technique.

CRediT authorship contribution statement

Yasin Heydarpour: Writing – review & editing, Writing – original draft, Formal analysis, Data curation. **Parviz Malekzadeh:** Writing – review & editing, Supervision, Conceptualization. **Hanxing Zhu:** Writing – review & editing, Supervision, Conceptualization. **Morteza Mohammadzaheri:** Writing – review & editing, Validation.

Declaration of competing interest

The authors declare that they have no known competing financial interests or personal relationships that could have appeared to influence the work reported in this paper.

Data availability

Data will be made available on request.

References

[1] Ray S, Loukou A, Trimis D. Evaluation of heat conduction through truncated conical shells. Int J Therm Sci 2012;57:183–91. https://doi.org/10.1016/j.ijthermalsci.2012.02.004.
[2] Wang YQ, Ye C, Zu JW. Nonlinear vibration of metal foam cylindrical shells reinforced with graphene platelets. Aerosp Sci Technol 2019;85:359–70. https://doi.org/10.1016/j.ast.2018.12.022.
[3] Qin Z, Pang X, Safaei B, Chu F. Free vibration analysis of rotating functionally graded CNT reinforced composite cylindrical shells with arbitrary boundary conditions. Compos Struct 2019;220:847–60. https://doi.org/10.1016/j.compstruct.2019.04.046.
[4] Qin Z, Shengnan Z, Xuejia P, Safaei B, Chu F. A unified solution for vibration analysis of laminated functionally graded shallow shells reinforced by graphene with general boundary conditions. Int J Mech Sci 2020;170:105341. https://doi.org/10.1016/j.ijmecsci.2019.105341.
[5] Liu Y, Qin Z, Chu F. Nonlinear forced vibrations of FGM sandwich cylindrical shells with porosities on an elastic substrate. Nonlinear Dyn 2021;104:1007–21. https://doi.org/10.1007/s11071-021-06358-7.
[6] Ye C, Wang YQ. Nonlinear forced vibration of functionally graded graphene platelet-reinforced metal foam cylindrical shells: internal resonances. Nonlinear Dyn 2021;104:2051–69. https://doi.org/10.1007/s11071-021-06401-7.
[7] Yang S, Hao Y, Zhang W, Yang L, Liu L. Nonlinear vibration of functionally graded graphene platelet-reinforced composite truncated conical shell using first-order shear deformation theory. Appl Math Mech 2021;42:981–98. https://doi.org/10.1007/s10483-021-2747-9.
[8] Liu Y, Qin Z, Chu F. Investigation of magneto-electro-thermo-mechanical loads on nonlinear forced vibrations of composite cylindrical shells. Commun Nonlinear Sci Numer Simul 2022;107:106146. https://doi.org/10.1016/j.cnsns.2021.106146.
[9] Gao Z, Shi X, Huang Z, Zhong R, Wang Q. Spectro-geometric solutions for random vibration of functionally graded graphene platelet reinforced conical shells. Thin Wall Struct 2024;195:111410. https://doi.org/10.1016/j.tws.2023.111410.
[10] Hong C-C. Thermal vibration of thick FGM conical shells by using third-order shear deformation theory. Materials 2024;17:2403. https://doi.org/10.3390/ma17102403.
[11] Parnian P, Shojaee M, Weeger O, D'Amore A. Multiscale modelling and characterisation of fused filament fabricated neat and graphene nanoplatelet reinforced G-polymers. Prog Addit Manuf 2024. https://doi.org/10.1007/s40964-024-00789-5.
[12] D.X. Luong, K.V. Bets, W.A. Algozeeb, M.G. Stanford, C. Kittrell, W. Chen, R. V. Salvatierra, M. Ren, E.A. McHugh, P.A. Advincula, Z. Wang, M. Bhatt, H. Guo, Vl. Mancevski, R. Shahsavari, B.I. Yakobson, J.M. Tour, Gram-scale bottom-up flash graphene synthesis, Nature 577 (2020) 647-51. https://doi.org/10.1038/s41586-020-1938-0.

[13] Kumar A, Sharma K, Dixit AR. A review on the mechanical properties of polymer composites reinforced by carbon nanotubes and graphene. Carbon Lett 2021;31: 149–65. https://doi.org/10.1007/s42823-020-00161-x.
[14] Jyoti J, Singh BP. A review on 3D graphene–carbon nanotube hybrid polymer nanocomposites. J Mater Sci 2021;56:17411–56. https://doi.org/10.1007/s10853-021-06370-7.
[15] Mousavi SR, Estaji S, Kiaei H, Mansourian-Tabaei M, Nouranian S, Jafari SH, et al. A review of electrical and thermal conductivities of epoxy resin systems reinforced with carbon nanotubes and graphene-based nanoparticles. Polym Test 2022;112: 107645. https://doi.org/10.1016/j.polymertesting.2022.107645.
[16] Razaq A, Bibi F, Zheng X, Papadakis R, Jafri SHM, Li H. Review on Graphene-. Graphene Oxide-, Reduced Graphene Oxide-Based Flexible Composites: from Fabrication to Applications, Materials 2022;15:1012. https://doi.org/10.3390/ma15031012.
[17] Etesami M, Nguyen T, Yonezawa A, Tuantranont A, Somwangthanaroj SK. 3D carbon nanotubes-graphene hybrids for energy conversion and storage applications. Chem Eng J 2022;446:137190. https://doi.org/10.1016/j.cej.2022.137190.
[18] P. Phani Prasanthi1, M.S.R. Niranjan Kumar, M. Somaiah Chowdary, V.V. Venu Madhav, K.K. Saxena, K.A. Mohammed, M.I. Khan, G. Upadhyay, S.M. Eldin, Mechanical properties of carbon fiber reinforced with carbon nanotubes and graphene filled epoxy composites: experimental and numerical investigations, Mater. Res. Express 10 (2023) 025308, DOI 10.1088/2053-1591/acaef5.
[19] Dutta T, Llamas-Garro I, Velázquez-González JS, Bas J, Dubey R, Mishra SK. A new generation of satellite sensors based on graphene and carbon nanotubes: A Review. IEEE Sens J 2024;24:31645–57. https://doi.org/10.1109/JSEN.2024.3440499.
[20] Shi G, Araby S, Gibson CT, Meng Q, Zhu S, Ma J. Graphene platelets and their polymer composites: fabrication, structure, properties, and applications. Adv Funct Mater 2018;28:1706705. https://doi.org/10.1002/adfm.201706705.
[21] García-Macías E, Rodríguez-Tembleque L, Sáez A. Bending and free vibration analysis of functionally graded graphene vs. carbon nanotube reinforced composite plates. Compos Struct 2018;186:123–38. https://doi.org/10.1016/j.compstruct.2017.11.076.
[22] Hussain M, Khan SM, Shafiq M, Al-Dossari M, Alqsair UF, Khan SU, et al. Comparative study of PLA composites reinforced with graphene nanoplatelets, graphene oxides, and carbon nanotubes: Mechanical and degradation evaluation. Energy 2024;308:132917. https://doi.org/10.1016/j.energy.2024.132917.
[23] Zhao S, Zhao Z, Yang Z, Ke L, Kitipornchai S, Yang J. Functionally graded graphene reinforced composite structures: A review. Eng Struct 2020;210:110339. https://doi.org/10.1016/j.engstruct.2020.110339.
[24] Yee K, Ghayesh MH. A review on the mechanics of graphene nanoplatelets reinforced structures. Int J Eng Sci 2023;186:103831. https://doi.org/10.1016/j.ijengsci.2023.103831.
[25] Wang YQ, Wan YH, Zhang YF. Vibrations of longitudinally traveling functionally graded material plates with porosities. Eur J Mech - A/solid 2017;66:55–68. https://doi.org/10.1016/j.euromechsol.2017.06.006.
[26] Babaei M, Asemi K, Safarpour P. Natural frequency and dynamic analyses of functionally graded saturated porous beam resting on viscoelastic foundation based on higher order beam theory. J Solid Mech 2019;11:615–34. https://doi.org/10.22034/jsm.2019.666691.
[27] M. Babaei, K. Asemi, P. Safarpour, Buckling and static analyses of functionally graded saturated porous thick beam resting on elastic foundation based on higher order beam theory, Iran. J. Mech. Eng. Trans. of ISME, 20 (2019) 94-112. 20.1001.1.16059727.2019.20.1.4.0.
[28] Babaei M, Asemi K. Stress analysis of functionally graded saturated porous rotating thick truncated cone. Mech Based Des Struct Mach 2020;50:1537–64. https://doi.org/10.1080/15397734.2020.1753536.
[29] Chai Q, Wang YQ. Traveling wave vibration of graphene platelet reinforced porous joined conical-cylindrical shells in a spinning motion. Eng Struct 2022;252: 113718. https://doi.org/10.1016/j.engstruct.2021.113718.
[30] Khatounabadi M, Jafari M, Asemi K. Low-velocity impact analysis of functionally graded porous circular plate reinforced with graphene platelets, Wave. Random Complex Media 2022:1–27. https://doi.org/10.1080/17455030.2022.2091182.
[31] Barbaros I, Yang Y, Safaei B, Yang Z, Qin Z, Asmael M. State-of-the-art review of fabrication, application, and mechanical properties of functionally graded porous nanocomposite materials. Nanotechnol Rev 2022;11:321–71. https://doi.org/10.1515/ntrev-2022-0017.
[32] Khatoonabadi M, Jafari M, Kiarasi F, Hosseini M, Babaei M, Asemi K. Shear buckling response of FG porous annular sector plate reinforced by graphene platelet subjected to different shear loads. J Comput Appl Mech 2023;54(1):68–86. https://doi.org/10.22059/jcamech.2023.352182.784.
[33] D. Chen, K. Gao, J. Yang, L. Zhang, Functionally graded porous structures: Analyses, performances, and applications-a review, Thin-Wall. Struct. 191 (2023) 191,111046. https://doi.org/10.1016/j.tws.2023.111046.
[34] Zhu J, Wang ZZ, Zhang L, Wu H, Zhao L, Zhang H, et al. Wave propagation in the semi-infinite functionally graded porous plates reinforced with graphene platelets. Int J Struct Stab Dy 2024;24:2450245. https://doi.org/10.1142/S0219455424502456.
[35] Bahranifard F, Malekzadeh P, Golbahar Haghighi MR. Moving load response of ring-stiffened sandwich truncated conical shells with GPLRC face sheets and porous core. Thin-Wall Struct 2022;180:109984. https://doi.org/10.1016/j.tws.2022.109984.
[36] Safaei M, Malekzadeh P, Golbahar Haghighi MR. Out-of-plane moving load response and vibrational behavior of sandwich curved beams with GPLRC face sheets and porous core. Compos Struct 2024;327:117658. https://doi.org/10.1016/j.compstruct.2023.117658.
[37] Bahranifard F, Malekzadeh P, Golbahar Haghighi MR, Żur KK. On the selected problems of time-dependent dynamics of composite truncated conical shells-like aerospace structures. Commun Nonlinear Sci Numer Simulat 2024;130:107717. https://doi.org/10.1016/j.cnsns.2023.107717.
[38] Liu T, Sun X, Hu WF, Wang L, Zhang S, Bui TQ. Nonlinear thermal-mechanical coupled isogeometric analysis for GPLs reinforced functionally graded porous plates. Eng Struct 2024;319:118827. https://doi.org/10.1016/j.engstruct.2024.118827.
[39] Amiri Delouei A, Emamian A, Sajjadi H, Atahafrooz M, Li Y, Wang LP, et al. Xie, A comprehensive review on multi-dimensional heat conduction of multi-layer and composite structures: analytical solutions. J Therm Sci 2021;30:1875–907. https://doi.org/10.1007/s11630-021-1517-1.
[40] Zhang Z, Sun Y, Zhou D, Gu Z, Gong H. Nonlinear transient heat transfer analysis of multilayered thermal protection systems by incremental differential quadrature element method. Case Studies in Therm Eng 2023;52:103730. https://doi.org/10.1016/j.csite.2023.103730.
[41] Jain A, Krishnan G, Hasrati E. A Heaviside functions based technique to solve multilayer transient thermal conduction problems. Int Commun Heat Mass 2024; 154:107323. https://doi.org/10.1016/j.icheatmasstransfer.2024.107323.
[42] Jain A, Krishnan G. Thermal spreading in a multilayer geometry with convective cooling along the side wall of each layer. Int Commun Heat Mass 2025;236: 126253. https://doi.org/10.1016/j.ijheatmasstransfer.2024.126253.
[43] Amiri Delouei A, Emamian A, Ghorbani S, He F. A general unsteady Fourier solution for orthotropic heat transfer in 2D functionally graded cylinders. Math Method Appl Sci 2024;47:3942–59. https://doi.org/10.1002/mma.9796.
[44] Tokovyy YV, Hrytsyna OR, Hrytsyna MR. Explicit thermal analysis of inhomogeneous multilayer cylinders using the direct integration method. Int J Therm Sci 2024;196:108654. https://doi.org/10.1016/j.ijthermalsci.2023.108654.
[45] Tokovyy YV. Stationary temperature fields in radially inhomogeneous hollow cylinders. Adv Struct Mat 2024;204:489–504. https://doi.org/10.1007/978-3-031-54063-9_31.
[46] Norouzi M, Rahmani H. On exact solutions for anisotropic heat conduction in composite conical shells. Int J Therm Sci 2015;94:110–25. https://doi.org/10.1016/j.ijthermalsci.2015.02.018.
[47] Norouzi M, Rahmani H. An exact analysis for transient anisotropic heat conduction in truncated composite conical shells. Appl Therm Eng 2017;124:422–31. https://doi.org/10.1016/j.applthermaleng.2017.06.039.
[48] Erfan Manesh B, Shahmardan MM, Rahmani H, Norouzi M. Heterogeneous anisotropic conductive heat transfer in composite conical shells: An exact analysis. Int J Heat Mass Tran 2019;144:118614. https://doi.org/10.1016/j.ijheatmasstransfer.2019.118614.
[49] Erfan Manesh B, Shahmardan MM, Norouzi M, Rahmani H. Unsteady anisotropic heat conduction in heterogeneous composite conical shells with temperature-dependent thermal conductivities: an analytical study. J Therm Anal Calorim 2022; 147:1773–92. https://doi.org/10.1007/s10973-020-10434-2.
[50] Heydarpour Y, Aghdam MM. A new multistep technique based on the nonuniform rational basis spline curves for nonlinear transient heat transfer analysis of functionally graded truncated cone. Heat Transfer Eng 2019;40:588–603. https://doi.org/10.1080/01457632.2018.1436422.
[51] Heydarpour Y, Malekzadeh P. Three-dimensional non-Fourier heat transfer analysis of multilayer functionally graded graphene platelets reinforced composite truncated conical shells. Heat Transfer Eng 2021;42:1303–18. https://doi.org/10.1080/01457632.2020.1785700.
[52] Huang Z, Dai H, Wei Y, Sun Z. Unsteady heat transfer in a multilayer composite cylinder containing porous media. Appl Therm Eng 2022;211:118425. https://doi.org/10.1016/j.applthermaleng.2022.118425.
[53] Duan X, Zhang W, Chi C, Li L, Jiang S, Chi G. Analysis of transient heat conduction within semi-infinite medium surrounding heated conical shell. Int J Therm Sci 2023;185:108028. https://doi.org/10.1016/j.ijthermalsci.2022.108028.
[54] Amiri Delouei A, Emamian A, Karimnejad S, Li Y. An exact analytical solution for heat conduction in a functionally graded conical shell. J Appl Comput Mech 2023; 9:302–17. https://doi.org/10.22055/JACM.2020.35641.2703.
[55] Mohammadlou V, Khoddami Maraghi Z, Ghorbanpour Arani A. Thermoelastic analysis of axisymmetric conical shells: Investigating stress–strain response under uniform heat flow with semi-coupled approach. Numer Heat Tr A-Appl 2024. https://doi.org/10.1080/10407782.2024.2326943.
[56] Chu K, Jia C, Li W. Effective thermal conductivity of graphene-based composites. Appl Phys Lett 2012;101:121916. https://doi.org/10.1063/1.4754120.
[57] K. Chu, C. C. Jia, W. S. Li, Erratum: "Effective thermal conductivity of graphene-based composites" [Appl. Phys. Lett. 101, 121916 (2012)], Appl. Phys. Lett. 101 (2012) 209902. .
[58] Eftekhari SA. A differential quadrature procedure with direct projection of the heaviside function for numerical solution of moving load problem. Lat Am J Solids Struct 2016;13:1763–81. https://doi.org/10.1590/1679-78252251.
[59] Malekzadeh P, Mohebpour SR, Heydarpour Y. Nonlocal effect on the free vibration of short nanotubes embedded in an elastic medium. Acta Mechanica 2012;223 (2012):1341–50. https://doi.org/10.1007/s00707-012-0621-4.
[60] Heydarpour Y, Aghdam MM, Malekzadeh P. Free vibration analysis of rotating functionally graded carbon nanotube-reinforced composite truncated conical shells. Compos Struct 2014;117:187–200. https://doi.org/10.1016/j.compstruct.2014.06.023.
[61] Hao Y, Sun L, Zhang W, Li H. Active traveling wave vibration control of elastic supported conical shells with smart micro fiber composites based on the differential quadrature method. Appl Math Mech-Engl Ed 2025;46:305–22. https://doi.org/10.1007/s10483-025-3216-7.

[62] Hao YX, Sun L, Zhang W, Li H, Li W, Yang SW. Study on the fundamental frequency and dynamic mode of traveling wave vibration of rotating PJCS. Int J Struct Stab Dyn 2024;24:2450280. https://doi.org/10.1142/S0219455424502808.
[63] Malekzadeh P, Rahideh H. IDQ two-dimensional nonlinear transient heat transfer analysis of variable section annular fins, Energ. Convers. Manage 2007;48:269–76. https://doi.org/10.1016/j.enconman.2006.04.005.
[64] Heydarpour Y, Aghdam MM. A coupled integral–differential quadrature and B-spline-based multi-step technique for transient analysis of VSCL plates. Acta Mechanica 2017;228:2965–86. https://doi.org/10.1007/s00707-017-1850-3.
[65] Heydarpour Y, Aghdam MM. Response of VSCL plates under moving load using a mixed integral-differential quadrature and novel NURBS based multi-step method. Compos, B Eng 2018;140:260–80. https://doi.org/10.1016/j.compositesb:2017.07.066.
[66] Heydarpour Y, Malekzadeh P. Thermoelastic analysis of multilayered FG spherical shells based on Lord–Shulman theory, IJST-T. Mech Eng 2019;43:845–67. https://doi.org/10.1007/s40997-018-0199-0.
[67] Heydarpour Y, Malekzadeh P, Gholipour F. Thermoelastic analysis of FG-GPLRC spherical shells under thermo-mechanical loadings based on Lord-Shulman theory. Compos Part B-Eng 2019;164:400–24. https://doi.org/10.1016/j.compositesb:2018.12.073.
[68] Heydarpour Y, Malekzadeh P, Dimitri R, Tornabene F. Thermoelastic analysis of rotating multilayer FG-GPLRC truncated conical shells based on a coupled TDQM-NURBS scheme. Compos Struct 2020;235:111707. https://doi.org/10.1016/j.compstruct.2019.111707.
[69] Heydarpour Y, Mohammadzaheri M, Ghodsi M, Soltani P, Al-Jahwari F, Bahadur I, et al. A coupled DQ-Heaviside-NURBS approach to investigate nonlinear dynamic response of GRE cylindrical shells under impulse loads. Thin-Wall Struct 2021;165:107958. https://doi.org/10.1016/j.tws.2021.107958.
[70] Heydarpour Y, Malekzadeh P, Zhu H. Three-dimensional response of multilayer FG-GPLRC spherical panels under blast loading. Inter J Struct Stab Dy 2022;22:2250111. https://doi.org/10.1142/S0219455422501115.
[71] Heydarpour Y, Malekzadeh P, Żur KK. Explosive blast loading effect on transient mechanical responses of aircraft panels with curvilinear fibers: 3D elasticity approach. Compos Struct 2024;334:117967. https://doi.org/10.1016/j.compstruct.2024.117967.
[72] Santos, Mota Soares H, Mota Soares CM, Reddy CAJN. A semi-analytical finite element model for the analysis of cylindrical shells made of functionally graded materials under thermal shock. Compos Struct 2008;86:10–21. https://doi.org/10.1016/j.compstruct.2008.03.004.
[73] Peng XL, Li XF. Thermal stress in rotating functionally graded hollow circular disks. Compos Struct 2010;92:1896–904. https://doi.org/10.1016/j.compstruct.2010.01.008.